SDSS Large Scale Structure Review

Ryan Scranton
University of Pittsburgh, PA 15206, USA

The recently completed Sloan Digital Sky Survey (SDSS) has proven to be a uniquely powerful and versatile resource for exploring late universe cosmology. The photometric survey has imaged over 7500 square degrees of the north Galactic cap in five filters streching from the near infrared to the near ultraviolet. Follow-up spectroscopy has been completed for nearly 750,000 galaxies, quasars and stars. This review covers three SDSS projects from the last year: measurement of the baryon signature in the spectroscopic survey, detection of weak gravitational lensing magnification bias in the photometric survey, and a preliminary application of weak lensing to characterize the relationship between cluster richness and mass.

1. INTRODUCTION

This talk reviewed three different large scale structure measurements made using the Sloan Digital Sky Survey (SDSS;Fukugita et al. 1996, Gunn et al. 1998, Smith et al. 2002) during the previous year. This review should not be taken as anything more than a brief introduction to the results of these measurements and their implications. Those who are interested in these results are strongly encouraged to read the original papers; nothing original will be presented in this review and numerous important details will omitted for the sake of brevity. In particular, this review will skip most of the references to previous work contained in those papers. Rather, we take our audience to be more along the lines of an interested non-astronomer, so we will concentrate on a more phenomenological description of what each measurement was trying to detect, how they went about it, and what they found.

2. SDSS BASICS

The SDSS is a large, homogeneous all-purpose survey, primarily covering the part of the sky coincident with the north Galactic cap. The observations are done using a dedicated 2.5 meter telescope located on Apache Point in the southwestern United States. First light was observed in late 1998 and the survey completed in summer of 2005. The SDSS can be thought of two surveys in one: a *photometric survey* mapping the sky across the optical region of the electromagnetic spectrum and a follow-up *spectroscopic survey* over that same region.

2.1. Photometric Survey

The photometric survey is done simultaneously across 5 optical bands: u, g, r, i and z, in order of increasing wavelength. The imaging is done using drift scanning, where the filters are arranged in columns on the telescope camera and the sky is allowed to drift along the line of filters concurrently. The SDSS camera has 6 of these scanline columns, separated by roughly 0.2°. When subsequent scans are interlaced to fill in their respective gaps, they form a imaging region roughly 2.5° wide. This associated pair of scans is referred to as a *stripe* and typically run between 90° and 120° degrees in length.

At the time of this talk, the fourth data release (DR4;Adelman-McCarthy et al. 2006) had just been made, covering an area of roughly 6670 square degrees and containing approximately 180 million objects. The survey has since been completed and the final data release, which increases the total area above 7500 square degrees, will be made in early summer 2006.

2.2. Spectroscopic Survey

After a region of the sky has been imaged by the photometric survey, a number of selection algorithms are applied to the associated data set to produce a list of targets for follow-up spectroscopy. This spectroscopy is done using two fiber-fed optical spectrographs mounted on the same 2.5 meter telescope. These spectrographs can observe 640 objects simultaneously. Typical exposures run for 45 minutes, so several thousand spectra can be taken in the course of one night.

The DR4 contained roughly 673,000 galaxy spectra, along with nearly 100,000 quasar and stellar spectra.

3. BARYON WIGGLES

The detection of baryon wiggles in the SDSS spectroscopic sample is described in Eisenstein et al. 2005. As stated above, all references to the relevant literature on acoustic oscilations can be found there.

The basic phenomenon here is the same one that produces the peaks in a cosmic microwave background (CMB) anisotropy experiment. The process begins at the time of matter-radiation equality, when the universe was roughly 10,000 times smaller than its current size (hence at a redshift, $z \sim 10,000$). Prior to this point in the history of the universe, the expansion was driven by the energy density of photons. Once matter took over as the dominant source of energy density, the initial perturbations in the distribution of energy left over from inflation were free to begin to collapse gravitationally.

While photons were no longer determining the expansion rate of the universe, they remained tightly bound to the matter distribution due to the prescence of baryons. As the baryons fell into the gravitational wells set up by the non-interacting (and dominant) dark matter, they pulled the photons along. This led to a series of oscilations in the plasma density as the photons would heat up during the compression phase and then cool off during the resultant rarefaction phase. Eventually, however, the universe cooled to the point that the photons were no longer energetic enough to ionize the baryons, the two species decoupled and the photons free-streamed through the universe. The imprint of the oscillations remained, however, leading to correlations in the temperature of the CMB radiation with a typical scale size corresponding to the radius of the largest scale that had enough time to reach the full compression phase just before decoupling. Since the baryons were oscillating in the same way, we should see a similar effect when we look at the clustering of galaxies, namely a spike in the correlation between galaxies at around 150 Mpc.

Cosmologically, this peak is a very valuable tool for determining the geometry of the universe. Like the CMB, this clustering peak is a standard ruler, a fixed angular scale at a given redshift that we can measure on the sky and compare to various cosmological models. Unlike the CMB, which is tied to the redshift of recombination, we can measure this scale for galaxies at a number of different points in the history of the universe. More immediately, the detection of this feature in the clustering of galaxies is an important comfirmation of our basic ideas about the creation of large scale structure in the universe.

3.1. Luminous Red Galaxies

The typical clustering length for galaxies is around 5 Mpc. This is equivalent to saying that we are roughly twice as likely to find galaxy pairs separated by 5 Mpc than we would expect to be if galaxies were randomly distributed throughout the universe. Since we are looking for galaxy pairs separated by distances roughly thirty times that distance we need a galaxy sample that is very uniform and one that encompasses a very large volume. The solution to both of these requirements is to use the SDSS Luminous Red Galaxy (LRG) sample.

LRGs are very large, very old galaxies that typically reside in the centers of very massive galaxy clusters. They typically have very little interstellar dust and no active star formation. Because they are more luminous than normal field galaxies, we can observe them at greater distances for a given magnitude limit and their stable colors make them relatively easy to pick out from the rest of the galaxies using the SDSS multi-band photometry. The LRG

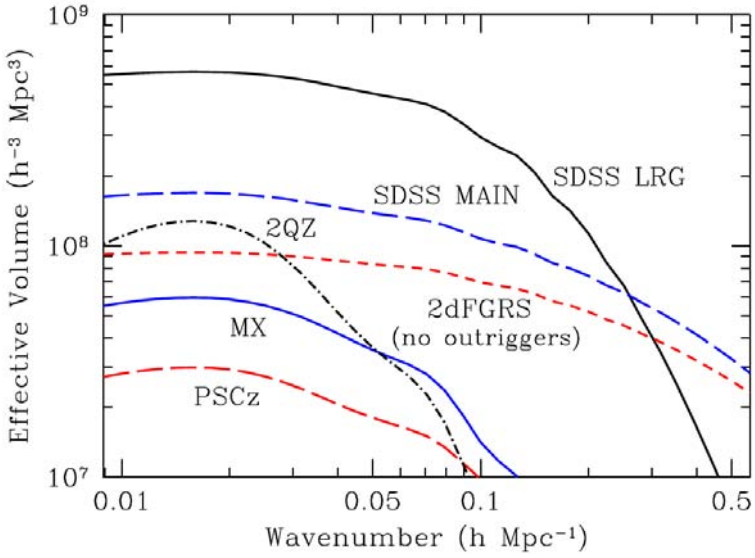

Figure 1: From Eisenstein et al. [2005], the effective volume of the SDSS LRG spectroscopic sample compared to other large spectroscopic surveys.

Table I: From Eisenstein et al. 2005, the cosmological constraints obtained from a combination of CMB anisotropies and SDSS main galaxy sample clustering and the constraints found when adding the baryon signature from the LRG clustering results. In all cases, a flat universe prior was assumed.

Parameter	**WMAP + SDSS Main**	**+ LRG**
w	-0.92 ± 0.30	-0.80 ± 0.18
$\Omega_M h^2$	0.145 ± 0.014	0.135 ± 0.008
Ω_m	0.329 ± 0.074	0.326 ± 0.037
h	0.679 ± 0.100	0.648 ± 0.045
n	0.984 ± 0.033	0.98 ± 0.035

sample used in this measurement contained roughly 47,000 galaxies spread throughout a volume of nearly 1 Gpc^3 (Figure 1), over 4 times that of the main SDSS galaxy sample.

3.2. Detection Results

The redshift space correlation function for the LRG sample is shown in Figure 2. As is clear in the inset, the clustering shows a clear spike at roughly 110 h^{-1}Mpc, right where we would expect it for a dark energy dominated universe. With the detection of this feature, we can improve a number of cosmological constraints, as shown in Table I. In particular, the errors on the dark energy equation of state (w) and the matter density (Ωh^2) are improved by a factor of 2 over those found with just measurements of the CMB anisotropies and the galaxy clustering from the SDSS main galaxy sample. Even more remarkable, when the prior for a flat universe is removed from the parameter constraints, the best fitting value for the curvature goes from $\Omega_K = -0.045 \pm 0.032$ to $\Omega_K = -0.010 \pm 0.009$ with the LRG measurements.

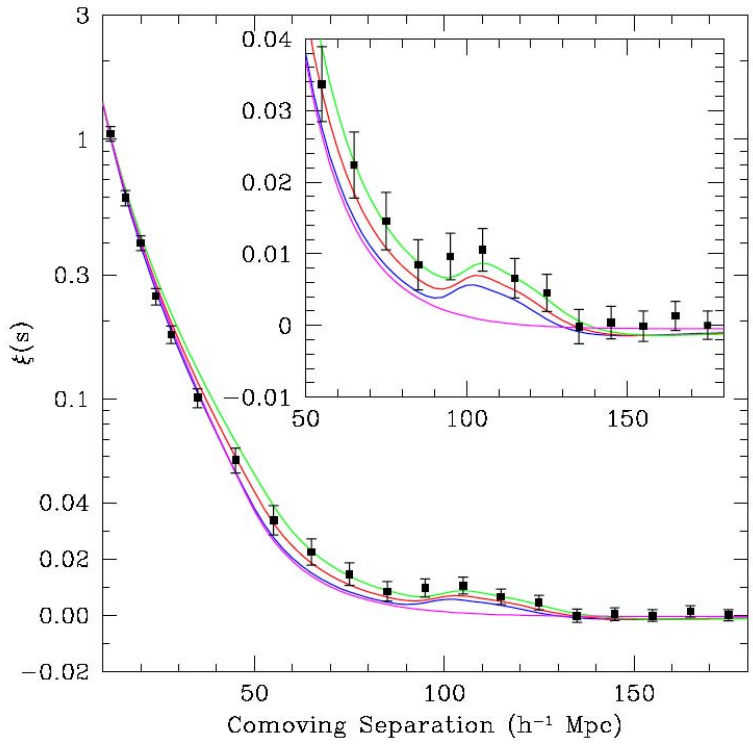

Figure 2: From Eisenstein et al. 2005, the redshift space correlation function for the LRG spectroscopic sample. For comparison, the expected curves for a number of flat ΛCDM universes are shown (from top to bottom): $\Omega_M h^2 = 0.12$, $\Omega_M h^2 = 0.13$, $\Omega_M h^2 = 0.14$ and a pure CDM model ($\Omega_M h^2 = 0.105$).

4. MAGNIFICATION BIAS

Magnification bias is the result of gravitational lensing, the bending of light as it passes through gravitational potentials on the way from a distant source to observers here on Earth. Specifically, magnification bias is a *weak lensing* effect where the alignment between source, lens and observer is not such that we see multiple images (as in strong lensing), but rather just a distortion of that light. Since this effect is small on an object by object basis, we need to look at many different sources and measure the average effect statistically.

The magnification of background sources by foreground lensing is actually two effects in one: amplification and dilution. First, because the foreground objects act as lenses, they tend to focus the photons from background sources, making them appear brighter than they would be normally. As such, if we are selecting our background sample based on their apparent brightness, then we would tend to see more of them near foreground objects since we would pick up a few extra objects that were normally below our threshold but made the cut thanks to being gravitationally lensed. The second effect comes from the fact that being gravitationally lensed deflects the apparent position of our background objects away from the foreground objects on the sky. As a result, the density of background objects should be smaller near the foreground objects.

Thus, the signal that we see when we correlate the density of foreground and background objects on the sky depends on the interaction of the amplification and dilution effects. If the number of objects that we pick up due to amplification is large relative to the number we lose due to dilution, then we will see a positive signal. Conversely, if amplification is not effective compared to dilution, then we will measure an anti-correlation between the two populations.

The motivation for doing this measurement is two-fold. First, different groups have been trying to detect this signal for roughly two decades. However, all previous attempts to measure the magnification bias have seen signals much larger than predicted by standard cosmological models. Second, this effect is very complentary to measurements of

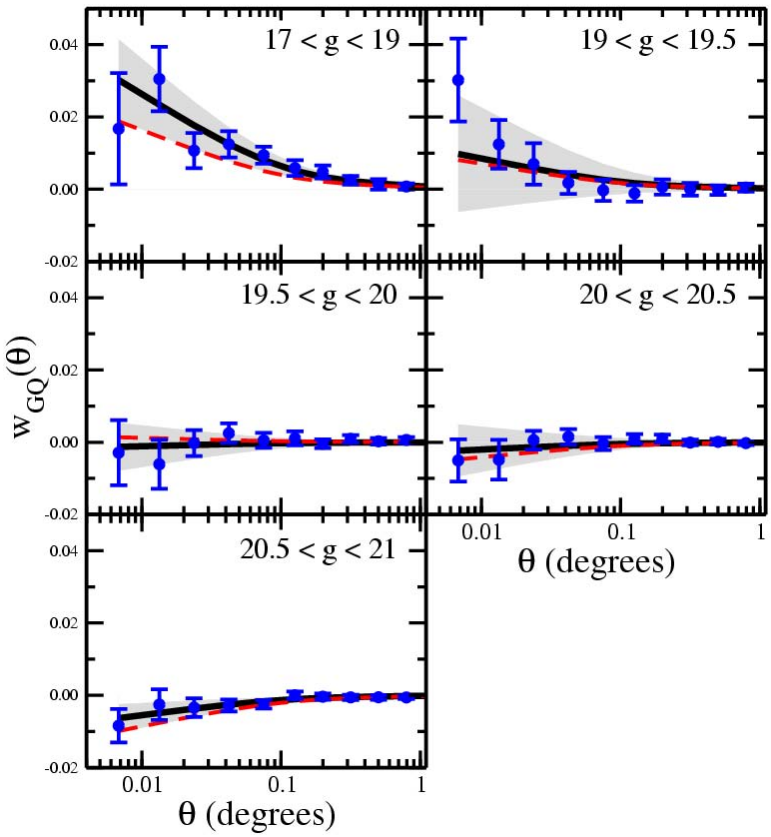

Figure 3: From Scranton et al. 2005, the magnification bias results. In each panel, the data points show the measured correlation, the dashed line the expected signal, the heavy solid line the best fitting model and the shaded region the 1σ error on that fit.

cosmic shear (see below), giving one the same cosmological information but with very different systematic errors. Thus, demonstrating that magnification bias can be reliably measured opens up an entire parallel track for all future weak lensing surveys.

4.1. Data

As mentioned above, magnification bias is a very subtle effect and detecting it requires very good control of both the systematic and statistical errors. For the latter, one must ensure that the foreground and background densities are not affected by external factors like observing conditions. Likewise, it is critical that the two populations are well separated in redshift so that the signal is not contaminated by clustering between the samples. On the statistical side, the dominant source of error comes from Poisson noise, so the samples need to be made as large as possible given all of the other constraints.

To measure this effect, we used galaxies and quasars drawn from the photometric survey. For the galaxy sample, we wanted to get a large, uniform sample at low redshift relative to our quasar sample, so we chose a simple magnitude cut in the r band: $17 < r < 21$. This gave us an average galaxy redshift around $z \sim 0.3$. For the quasars, we used a kernel density estimator technique to select the largest sample of quasars ever assembled. From this sample, we applied photometric redshift cuts to bring us down to roughly 100,000 quasars all of which had redshifts above unity.

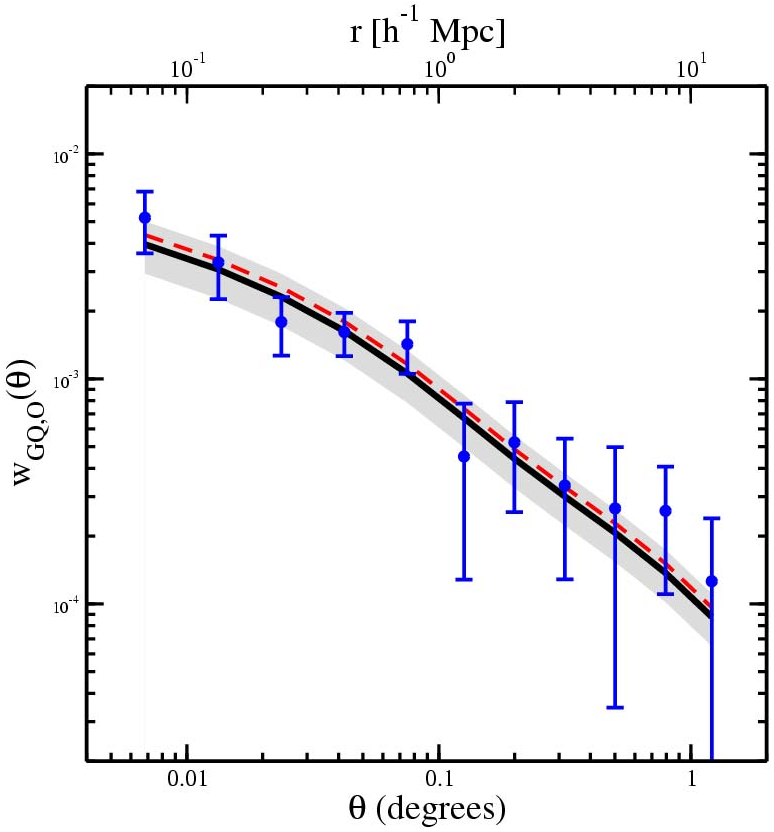

Figure 4: From Scranton et al. 2005, the magnification bias using the optimal estimator.

4.2. Results

To measure this effect, we split our quasar sample into 5 sub-samples, selected by magnitude. For each sub-sample, we predicted the expected signal for the magnification bias based on the balance between the amplification and dilution signals. The basic trend was that, for bright quasars, we expected to see a positive correlation, while faint quasars should be anti-correlated with our foreground galaxies. As shown in Figure 3, this is precisely what we observed, with the measured signal matching both the amplitude, angular variation and change in sign predicted by the theory.

While this is a clear demonstration of the expected magnification signal, it is not the optimal way to do so. Ideally, one would like to combine all of the quasars into a single measurement and extract the full statistical power of the data set. Unfortunately, the expected signal for the full quasar sample is very close to zero. However, by weighting each quasar by the expected lensing signal, we can coherently add the signal from the faint quasars to the bright quasars instead of having them cancel each other. The result of this exercise is shown in Figure 4. This is an 8σ detection of magnification bias.

5. CLUSTER LENSING

As mentioned during the talk, the results in this section are still preliminary. Details will be provided in Sheldon et al. [2006] and the basic results should remain the same, but this should not be taken as the final word on these measurements.

Like the magnification bias, we are again looking at a weak lensing effect, although this is the more familar *shear effect*. If the background sources that we are observing are resolved objects like galaxies, then the effect of passing near

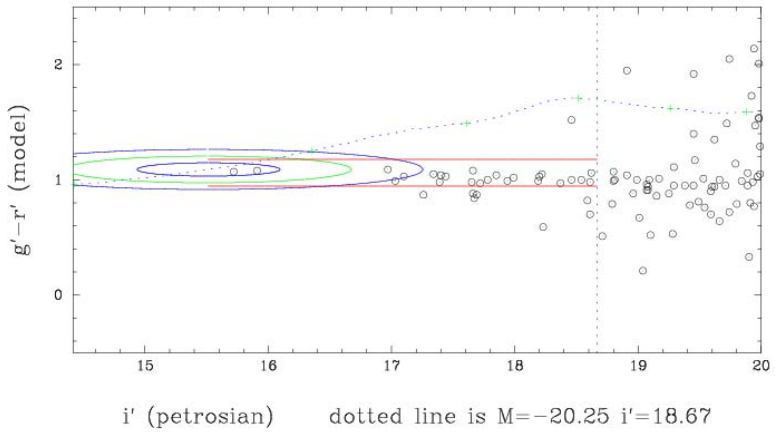

Figure 5: From Jim Annis, the color-magnitude evolution of MaxBCG galaxies as a function of redshift. One finds galaxies clusters by locating nearby fainter galaxies with the same color.

a foreground object's gravitational potential will tend to distort the background image in the direction perpendicular to the gradient of the potential (roughly tangential to a circle centered on the foreground object). Measurements of weak lensing using this shear have been done using large galaxy clusters, individual galaxies (statistically stacked on top of each other like with the magnification bias) and large scale structure, also known as *cosmic shear*. For this measurement, we are doing a combination of the first two: measuring the shear around galaxy clusters, but taking the average of many, many clusters so that we can get a better measurement of the average density for these clusters as a function of radius.

For almost a decade now, computer simulations of dark matter clustering have found that the dark matter halos which would host galaxy clusters like the ones mentioned above have a very distinct variation of density with radius, an NFW profile (after Navarro, Frenk and White, who first described this behavior) with a shallow power law slope at small radii giving way to a $1/r^3$ distribution at large radii. Properly scaled, this NFW profile appears to be more or less consistent regardless of halo mass in the simulations. By making measurements of the shear at a number of different radii for a wide range of cluster masses, we can directly test the NFW profile for the first time.

5.1. Cluster Catalog

To find the clusters to serve as our lenses, we used the MaxBCG method. The basis for this selection algorithm is the fact that if you take the brightest galaxy from any given galaxy cluster, it will tend to have basically the same color as all of the other brightest cluster galaxies at that redshift. Like the LRGs (which tend to be brightest cluster galaxies), these galaxies have a very well behaved variation in color with redshift. Finally, there will also be a number of other fainter galaxies in the cluster with the same color. Thus, one can find these galaxy clusters by looking for galaxies on the color-evolution track shown in Figure 5 and then finding other fainter, similarly colored galaxies within some fiducial radius.

Applying this method to the DR4 data set yields 600,000 "clusters", where the number of galaxies is ≥ 2. For a more stringent definition of "cluster" ($N \geq 10$), there are roughly 10,000 members.

5.2. Detection

With our cluster catalog in hand, we can measure the shear of background galaxies relative to the centers of each galaxy cluster. Figure 6 shows the results when the total cluster sample is separated into bins based on the number of galaxies in the lensing cluster. Two things are evident from this figure. First, there is a clear trade-off in the signal-to-noise between the relatively weak but plentiful small mass halos and the stronger but scarcer high

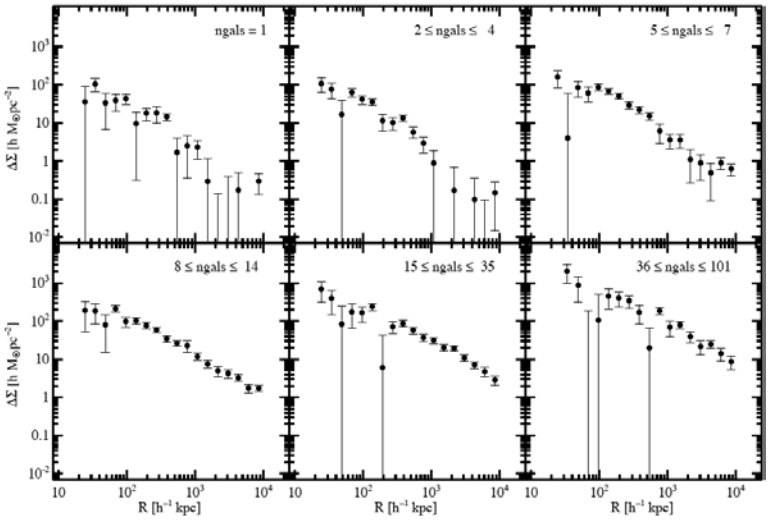

Figure 6: From Sheldon et al. 2006, weak lensing shear as a function of cluster richness.

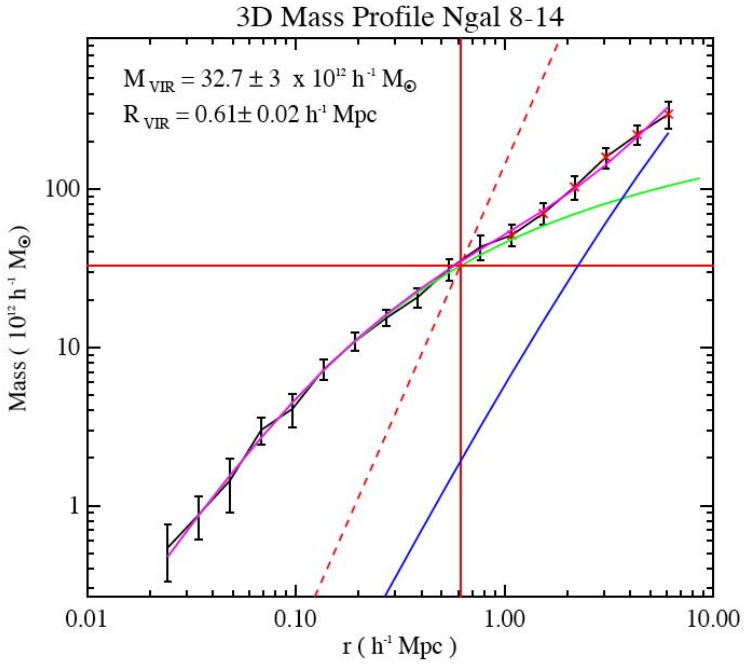

Figure 7: From Sheldon et al. 2006, fitting the NFW profile against the mass inferred from the lensing shear in the $8 < N_{gals} < 14$ richness bin. The green line is the NFW profile, the blue line is the contribution from nearby halos and the magenta line is the sum of the two.

mass halos, with the best signal-to-noise coming in the intermediate range. Second, and more important, the basic prediction of a single typical mass profile as seen in the simulation appears to be reflected in the data. This is made more even explicit in Figure 7 where the NFW profile is fit to the data, providing an excellent match.

Acknowledgments

Funding for the creation and distribution of the SDSS Archive has been provided by the Alfred P. Sloan Foundation, the Participating Institutions, the National Aeronautics and Space Administration, the National Science Foundation, the U.S. Department of Energy, the Japanese Monbukagakusho, and the Max Planck Society. The SDSS Web site is http://www.sdss.org/.

The SDSS is managed by the Astrophysical Research Consortium (ARC) for the Participating Institutions. The Participating Institutions are The University of Chicago, Fermilab, the Institute for Advanced Study, the Japan Participation Group, The Johns Hopkins University, the Korean Scientist Group, Los Alamos National Laboratory, the Max-Planck-Institute for Astronomy (MPIA), the Max-Planck-Institute for Astrophysics (MPA), New Mexico State University, University of Pittsburgh, University of Portsmouth, Princeton University, the United States Naval Observatory, and the University of Washington.

References

Adelman-McCarthy, J.K., et al. 2006, ApJS, 162, 38
Eisenstein, D.J., et al. 2005, ApJ, 633, 560
Fukugita, M., Ichikawa, T., Gunn, J.E., Doi, M., Shimasaku, K., and Schneider, D.P. 1996, AJ, 111, 1748
Gunn, J.E., et al. 1998, AJ, 116, 3040
Scranton, R., et al 2005, ApJ, 633, 589
Sheldon, E., et al 2006, *in preparation*
Smith, J.A., et al 2002, AJ, 123, 2121